UROP Logbook

D.Ezaz

September 15, 2022

1 Intro

This serves as the logbook for the work done on my UROP of 2022. It is based of the work done by Samuel Adams in the second year of his PhD [1]. The project started off working with the analytic cases in order to gain familiarity with the problem, before moving onto finite differences and progressively modelling increasingly complicated situations.

2 Methods and Results

2.1 Analytic case

2.1.1 Scattering by hard cylinder

The analytic case is particularly easy to solve. It involves solving the Helmholtz equation in cylindrical coordinates via separation of variables. The angular part of the solution gives rise to Bessel function modes, which must be summed over to achieve a general solution, much like obtaining trigonometric functions from other common DEs. The radial part gives a similar contribution to the final solution. After carrying out the necessary far field expansions, the expression for the far field scattered pressure is (more details on the derivation can be found in pages 92 onwards of [3])

$$\begin{aligned} p_{sf}(r,\phi,z) = -A\sqrt{2/\pi kr\sin\theta_i}\exp\left(\mathrm{i}kr\sin\theta_i\right)\exp(-\mathrm{i}\pi/4)\times \\ \exp\left(-\mathrm{i}kz\cos\theta_i\right)\sum_{n=-\infty}^{\infty}(-1)^{|n|}\frac{\mathrm{J}'_{|n|}(ka\sin\theta_i)}{\mathrm{H}'_{|n|}(ka\sin\theta_i)}\exp\left(\mathrm{i}n\left(\phi-\phi_i\right)\right). \end{aligned} \tag{1}$$

Obtaining the directivity involves factoring out the cylindrically spreading wave part - i.e $(1/\sqrt{r\sin\theta_i})\exp ikr\sin\theta_i$. The result of truncating this series to 150 terms, and plotting in python is shown in figure 1. This is consistent with code written by Samuel Adams, which is shown in figure 2.

Figure 1: The analytic far field directivity for the hard cylinder of radius unity. Non-dimensional wavenumber is 6, the radius of the cylinder is unity and the incident angle of the field is pi radians

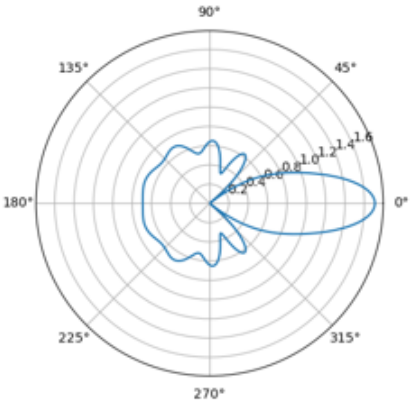

Figure 2: The numerical far field directivity for the hard cylinder of radius unity produced by Samuel Adam's code [1].

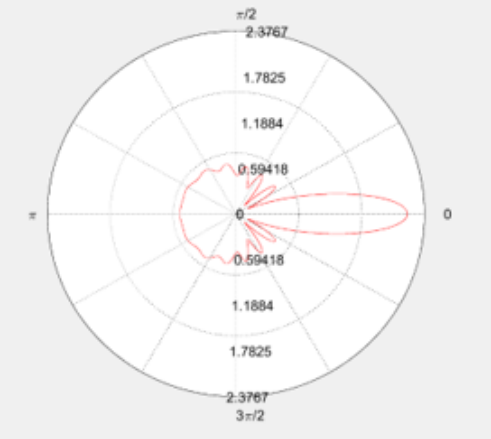

2.1.2 Scattering by soft cylinders

The scattering for soft cylinders proceeds very similarly to that of hard cylinders. The real difference lies in the "boundary conditions". When the cylinder is soft, the total pressure on the surface is required to vanish. In constrast, the acoustic particle displacement is required to vanish on the boundary for the hard case [3]:

$$W_r(r=a,\phi,z) = \frac{1}{\rho\omega^2}\frac{\partial p(r,\phi,z)}{\partial r}\bigg|_{r=a} = 0 \tag{2}$$

Once the correct BC is applied for the soft case, the scattered far field pressure is found to be [3]

$$\begin{aligned} p_{sf}(r,\phi,z) = &-A\sqrt{2/\pi kr\sin\theta_i}\exp\left(\mathrm{i}kr\sin\theta_i\right)\exp(-\mathrm{i}\pi/4)\times \\ &\exp\left(-\mathrm{i}kz\cos\theta_i\right)\sum_{n=-\infty}^{\infty}(-1)^{|n|}\frac{\mathrm{J}_{|n|}\left(ka\sin\theta_i\right)}{\mathrm{H}_{|n|}\left(ka\sin\theta_i\right)}\exp\left(\mathrm{i}n\left(\phi-\phi_i\right)\right). \end{aligned} \tag{3}$$

Implementing this in a similar way, the directivity pattern is shown in figure 3

Figure 3: The analytic far field directivity for the soft cylinder with the same parameters used for the hard cylinder in figure 1.

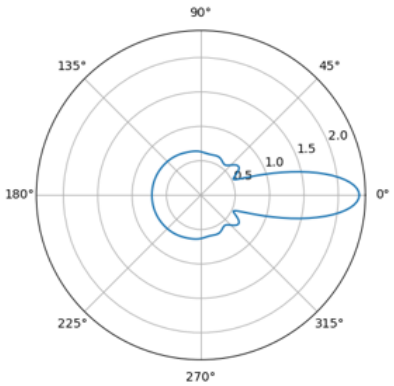

2.2 Moving onto finite differences

The next part considers using finite differences to solve the scattering problems. Care was taken in choosing the gridding scheme. The general idea is shown in 4, and the number of points dynamically allocated using 16.5 points per wavelength.

Figure 4: The general gridding scheme. Spacing may be non-linear. Obtained from [2]

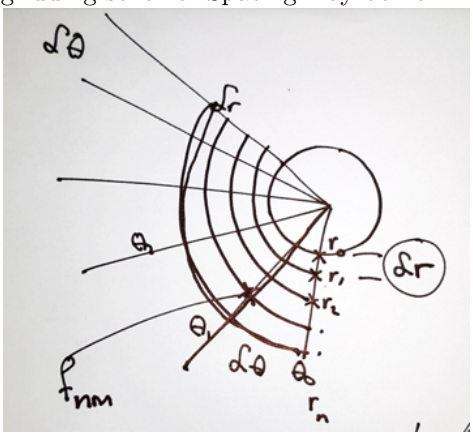

2.2.1 Scattering by hard cylinder

The start of the problem is deciding on the coordinate scheme, which is shown in figure 5. There is a need to truncate the domain. In doing so, one introduces a boundary by which numerical reflection can occur, which would cause an extra contribution to any pressure you are calculating. The approach is to use a perfectly matched layer (PML), which is wrapped around the domain of interest. It absorbs the "energy" of the wave, meaning that by the time the wave meets the far boundary of the PML in order to reflect, its energy is sufficiently small to have little contribution to the pressure. A PML is implemented by introducing the following coordinate transform [1]:

$$\begin{aligned} r \to r + \tfrac{\mathrm{i}}{\omega}\int_{r_B}^{r}\alpha(s)\mathrm{ds}, \quad \tfrac{\partial}{\partial r} \to \tfrac{1}{S}\tfrac{\partial}{\partial r}, \\ h_\theta \to r + \tfrac{\mathrm{i}}{\omega}\int_{r_B}^{r}\alpha(s)\mathrm{d}, \text{ where } S(r) = 1 + \tfrac{\mathrm{i}\alpha(r)}{\omega} \\ \alpha(r) = \alpha_{\max}\left(r - r_B\right)^2 / \left(r_P - r_B\right)^2, \end{aligned} \tag{4}$$

Where h_θ is the coordinate scale factor for the angular variable. Deciding on the parameters of the PML, for instance α_{max} is semi-empirical, but I used the parameters as tuned by Samuel Adams [1]. This corresponds to a PML that is 3 wavelengths in long, and $\alpha_{max} = 1$. After applying the PML, the new equation for the dynamics becomes

$$\frac{1}{S^2}\frac{\partial^2\phi_B}{\partial r^2} + \left(\frac{1}{h_\theta S} - \frac{1}{S^3}\frac{\mathrm{d}S}{\mathrm{d}r}\right)\frac{\partial\phi_B}{\partial r}\frac{1}{h_\theta^2 S}\frac{\partial^2\phi_B}{\partial\theta^2} + \left(\eta_B\omega\right)^2\phi_B = 0, \tag{5}$$

which reduces to the non-PML choice with the choice of boundary conditions used in [1]. The last issue is discretising the equation. This essentially involves deriving differential operators, in our case using the method of Fornberg and a five point differencing scheme. The Kronecker products are taken between the matrices and an identity matrix in order to promote them to the correct size. A total matrix operator is then formed form combining these matrices and the correct $1/r$ type factors. This is done for the fluid and also the PML, and the results stacked upon one another to make one big matrix that can solve for the entire physical space. Care must be taken when at the boundaries of particular regions, since one might need to use a forward or backwards differencing scheme instead of the typical central differencing used. More details of this can be found in the code. The solution is obtained by inverting the matrix, but only after the correct boundary conditions have been applied to fill out the necessary elements. Again, comments in the code explain this more.

Figure 5: The cylinder is of radius unity, so spans $0 < r < 1$. The background fluid spans $1 < r < r_B$ and the PML from $r_B < r < r_P$ [2]

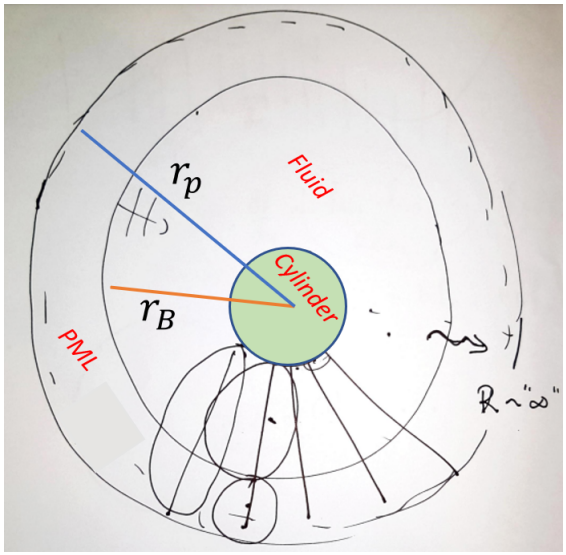

The field pressure is shown as a colourmap in 6. This compares well to figure 2 which shows the corresponding colourmap from the MATLAB code.

Figure 6: The colourmap for the simulation

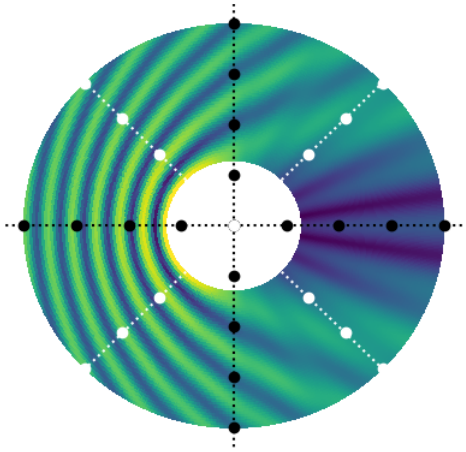

Figure 7: The corresponding colourmap to figure 6

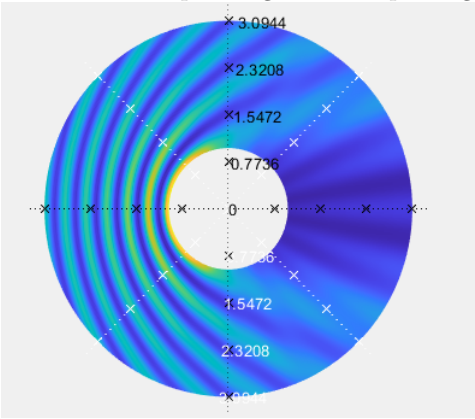

2.2.2 Empty submerged hard cylinder

This case is similar to the hard cylinder, but extra care must be taken. This case required solving the Helmholtz equation twice - one for shear waves and another for compressional waves [2]:

$$\nabla^2\phi + \frac{\omega^2}{c_d^2}\phi = 0 \qquad \nabla^2\phi + \frac{\omega^2}{c_s^2}\phi = 0 \tag{6}$$

Additionally, extra boundary conditions make the situation more difficult. These are shown in detail in figure 8

Figure 8: Diagram for the case being considered. Red ink denotes the new boundary conditions at play.

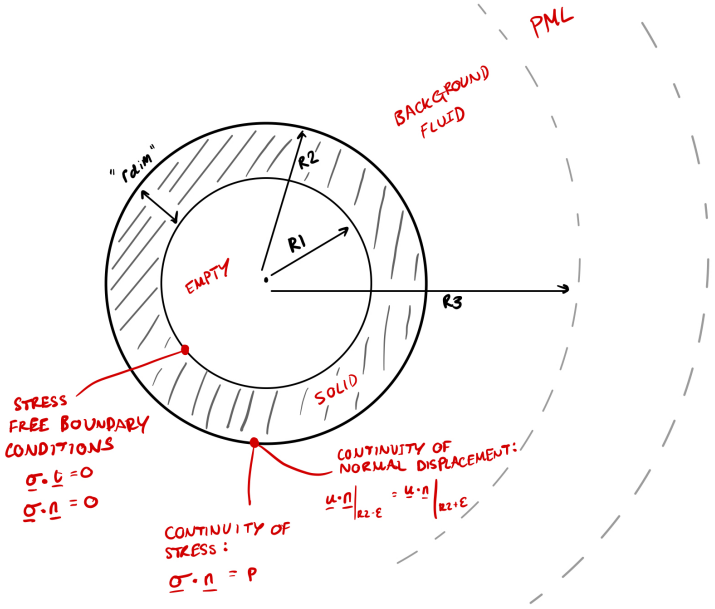

Another point to mention is obtaining the far field directivity once the solution around the boundary of the annulus is found. Greens theorem is used here, namely [1]

$$\phi_{BS}\left(r_0,\theta_0\right) = \int_0^{2\pi}\left(G\frac{\partial\phi_{BS}}{\partial r} - \phi_{BS}\frac{\partial G}{\partial r}\right)\Bigg|_{r=1}\mathrm{d}\theta, \tag{7}$$

where G is the 2D free space Green's function and ϕ_{BS} is the scattered directivity. This means if we know the scattered directivity at $r = 1$, and can also calculate the derivative, then we can work outwards and find the solution at some point (r_0, θ_0). This was done practically by using the trapezium rule. The result in the far field limit is shown in figure 9, and is consistent with what one would expect.

Figure 9: The far field directivty for an incident plane wave of angle $\pi/3$

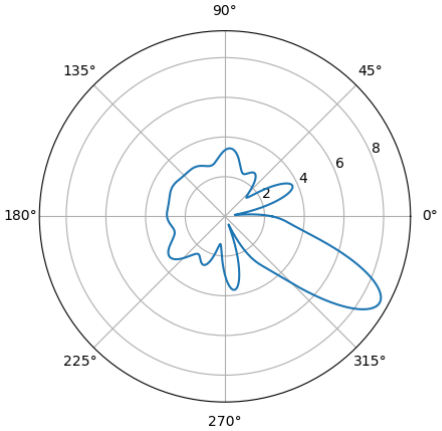

In many situations real-world situations, it would be impractical to measure the reflected directivity around an entire object. Instead, one would like to stand in a fixed position and use the back scattering for different frequencies to make deductions about the object. With slight - albeit shoddy - modification, this can be simulated with the code. Simulations take a while to run, as it involves re-running the dynamics over and over, but a typical result can be seen in

3 Code availability

The code for this report is available at https://github.com/dae1819/Dan-UROP-2022

References

[1] S.D.M Adams. *Asymptotic and numerical methods for surface waves and modes in elastic guiding structures*. PhD thesis, Imperial college London, 2009.

[2] R.V Craster. Personal communication.

[3] E.A. Skelton and J.H. James. *Theoretical Acoustics of Underwater Structures*. Imperial College Press, 1997.